HHS Public Access

Author manuscript

ACS Chem Biol. Author manuscript; available in PMC 2021 June 19.

Published in final edited form as:

ACS Chem Biol. 2020 June 19; 15(6): 1340–1348. doi:10.1021/acschembio.0c00308.

Hydrocarbon-stitched Peptide Agonists of Glucagon-Like Peptide-1 Receptor

Gregory H. Bird[1,2,*], **Accalia Fu**[3,4], **Silvia Escudero**[1,2], **Marina Godes**[1,2], **Kwadwo Opoku-Nsiah**[1,2], **Thomas E. Wales**[5], **Michael D. Cameron**[6], **John R. Engen**[5], **Nika N. Danial**[3,7,8], **Loren D. Walensky**[1,2,*]

[1]Department of Pediatric Oncology, Dana-Farber Cancer Institute, 450 Brookline Avenue, Boston MA, 02215

[2]Linde Program in Cancer Chemical Biology, Dana-Farber Cancer Institute, 450 Brookline Avenue, Boston MA, 02215

[3]Department of Cancer Biology, Dana-Farber Cancer Institute, 450 Brookline Avenue, Boston MA, 02215

[4]Department of Cell Biology, Harvard Medical School, Harvard Medical School, 240 Longwood Ave., Boston, MA 02115

[5]Department of Chemistry and Chemical Biology, Northeastern University, 360 Huntington Ave., Boston, MA 02115

[6]DMPK Core, Department of Molecular Medicine, 130 Scripps Way, The Scripps Research Institute, Jupiter, FL, 33458

[7]Department of Medical Oncology, Dana-Farber Cancer Institute, 450 Brookline Ave., Boston, MA, 02215

[8]Department of Medicine, Harvard Medical School, 240 Longwood Ave., Boston, MA, 02115

Abstract

Glucagon-like peptide 1 (GLP-1) is a natural peptide agonist of the GLP-1 receptor (GLP-1R) found on pancreatic β-cells. Engagement of the receptor stimulates insulin release in a glucose-dependent fashion and increases β-cell mass, two ideal features for pharmacologic management of type 2 diabetes. Thus, intensive efforts have focused on developing GLP-1-based peptide agonists of GLP-1R for therapeutic application. A primary challenge has been the naturally short half-life of GLP-1 due to its rapid proteolytic degradation *in vivo*. Whereas mutagenesis and lipidation

[*]**Corresponding Authors:** Loren_Walensky@dfci.harvard.edu, Greg_Bird@dfci.harvard.edu.

Author Contributions

G.H.B. and L.D.W. conceived of and designed the study. G.H.B. synthesized the peptide constructs. S.E. generated the GFP-GLP-1R expressing U2OS cell line. G.H.B., M.G. and K. O.-N. performed the receptor internalization assays. G.H.B. conducted the CD, cAMP, and *in vitro* proteolysis analyses. T.E.W. and J.R.E. conducted the HXMS analyses. M.D.C. performed the *ex vivo* plasma stability testing. G.H.B. and M.G. performed the *in vivo* experiments with the guidance of A.F. and N.D.D. G.H.B. and L.D.W. wrote the paper, which was reviewed by all co-authors.

Supporting Information includes GLP-1R internalization assay biological replicate data, cAMP assay, semaglutide proteolysis, HPLC profiles of stapled and stitched GLP-1 peptides, and a table of peptides generated, their masses, and use by figure. This material is available free of charge via the Internet at http://pubs.acs.org.

L.D.W. is a scientific cofounder and shareholder in Aileron Therapeutics.

strategies have yielded clinical agents, we developed an alternative approach to preserving the structure and function of GLP-1 by all-hydrocarbon *i, i+7* stitching. This particular “stitch” is especially well-suited for reinforcing and protecting the structural fidelity of GLP-1. Lead constructs demonstrate striking proteolytic stability and potent biological activity *in vivo*. Thus, we report a facile approach to generating alternative GLP-1R agonists for glycemic control.

Graphical Abstract

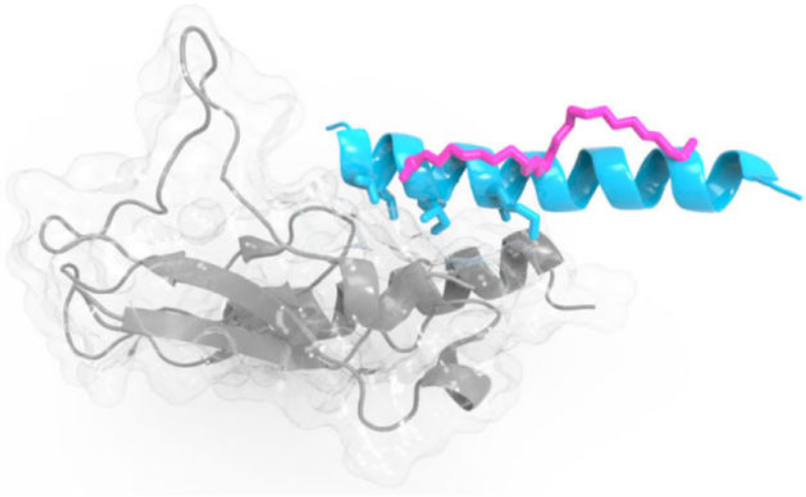

Keywords

Stapled Peptide; Stitched Peptide; GLP-1; GLP-1 Receptor; Hyperglycemia; Diabetes

INTRODUCTION

Peptide hormones regulate a myriad of biological activities, rendering their pharmacologic mimetics high priority agents for clinical development. A cardinal example is the chemical iteration of glucagon-like peptide 1 receptor (GLP-1R) agonists based on the amino acid sequences of glucagon-like peptides from humans and other species.[1, 2] Classic drawbacks of peptide drugs include loss of structure, particularly when required for biological activity, and the proteolytic lability of the peptide amide bond. Numerous approaches have been applied to overcome these barriers, including the use of non-natural and D-amino acids to replace labile sequences, and derivatizing peptides with PEG, lipids, or other moieties to improve pharmacokinetic properties.[3–13] Insertion of all-hydrocarbon staples has emerged as an effective strategy for both restoring α-helical shape to bioactive peptide helices and conferring substantial proteolytic resistance, properties that have facilitated their translation as *bona fide* therapeutic candidates.[14–20] One such example is an *i, i+7*-stapled peptide modeled after the p53 transactivation helix that naturally targets two negative regulators of the p53 pathway, HDM2 and HDMX.[21, 22] By neutralizing these targets, stapled p53 peptides can restore p53-mediated apoptosis in chemoresistant cancers and are currently being tested in adult and pediatric clinical trials.[23, 24]

A variety of stapling strategies have now been described, including single and double crosslinks that span one- or two-turns of an α-helix, and a stitching method whereby amino acid.[15, 17–19, 25] A single *i, i+7*- and a double *i, i+4* -stapled peptides have been advanced to clinical testing (NCT02264613, NCT03654716, NCT01775358). To date, stitching has not been vetted in a biological or therapeutic context. A key consideration in designing stapled peptides is selecting the ideal crosslink type to recapitulate the native alpha-helical structure of interest. For example, in attempting to develop immunogens that mimic the helix-kinkhelix of the membrane proximal external region (MPER) of the HIV-1 gp41 protein, we discovered that installing *i, i+3* and *i, i+4* crosslinks in the helical regions of the peptide optimally restored the native structure.[26] Whereas double *i,i+4* staples conferred ideal properties to the HR2 domain peptide of HIV-1 to yield a potent HIV-1 fusion inhibitor that overcame mutation-based resistance, double *i, i+7* staples were optimal for developing an RSV fusion inhibitor based on the homologous RSV-F HR2 domain sequence.[17, 19] For short peptides, single staples are typically sufficient, such as the single *i, i+4* staple applied to BCL-2 family BH3 domain helices or the single *i, i+7* staple installed in the p53 transactivation peptides, but longer constructs benefit from the extended structural reinforcement and proteolytic fortification afforded by double staples or stitches.[15, 17–19, 22, 27–35]

The helical structure of GLP-1 agonist peptides make these templates logical candidates for stapling, and indeed we previously demonstrated that *i, i+4* double-stapling of exendin-4 (Byetta) conferred structural and proteolytic stability.[17] Single staples generated by dithiol bis-alkylation and bearing various PEG-based serum-binding motifs, have also been used to stabilize exendin-4 and GLP-2 peptides for potential applications in diabetes and inflammatory bowel disease, respectively.[36, 37] The application of double-click helix stabilization chemistries to exendin-4 has also yielded compounds for imaging GLP-1R and with improved pharmacologic properties.[38, 39] The development of GLP-1 agonists such as semaglutide for clinical use, based on amino acid mutagenesis to avoid N-terminal proteolysis and lipid derivatization to enhance serum binding and thus circulatory half-life, has been remarkably successful.[40–42] Here, we sought to determine if stapling could yield alternative GLP-1 therapeutic candidates by use of a streamlined stapling design and validation workflow. Indeed, a standardized approach to generating high-fidelity structures that resist proteolysis could usher in a new generation of stapled peptide hormone drugs.

RESULTS AND DISCUSSION

The helical structure of the biologically-active GLP-1 peptide is comprised of an N-terminal segment that sits deep within the GLP-1R binding pocket and a C-terminal portion that participates in a more traditional helix-in-groove interaction with the extracellular domain of GLP-1R (Figure 1a).[43–45] Given the 30-amino acid length of GLP-1 peptide agonists, we initiated our design workflow by synthesizing an *i, i+7* staple scanning library of GLP-1 in an effort to maximize the umbrella of proteolytic protection (Figure 1b, Supplementary Table 1). To our knowledge, this is the first example of a systematic exploration of all possible *i, i+7* staple positions within an alpha-helical peptide hormone such as GLP-1 to interrogate structure-activity relationships (SAR). To rapidly screen our stabilized alpha-helices of GLP-1 (SAH-GLP-1) constructs for functional GLP-1R binding activity, we

generated U2OS cells (chosen based on the absence of endogenous, competing GLP-1R) that stably express GFP-GLP-1R and upon receptor engagement by GLP-1 undergo internalization of the complex, which can be detected and quantified rapidly by high-content epifluorescence microscopy (Figure 1c–d, Supplementary Figure 1a). Using a screening dosing regimen designed to capture a broad range of activity (0.625–10 μM), we evaluated each *i,i+7*-stapled GLP-1 peptide in the GLP-1R internalization assay. The screen uncovered three striking structure-function principles. First, nine of the ten N-terminal staple positions were not compatible with GLP-1R binding and internalization (Figure 1e, Supplementary Figure 1b). These data are consistent with the requisite burial of the peptide N-terminus in the receptor and the staple producing steric hindrance or replacing residues critical to agonistic function (Figure 1a). Second, tolerance of staples at up to five consecutive positions within the extracellular domain-binding portion of GLP-1, namely from 16,23 through 20,27, indicated that no discrete surface in this region is essential to inducing GLP-1R internalization (Figure 1e, Supplementary Figure 1b). Third, consecutive pairs of heptads situated along the length of the GLP-1 helix (e.g. 16,23/23,30; 17,24/24,31; 18,25/25,32; 19,26/26,33) showed patterns of tolerability for receptor engagement (Figure 1e–f), suggesting that long-range α-helical reinforcement might be best accomplished in this case by double *i, i+7* "stitching"[25], which affords a common bridging point for the two staples (Figure 2a) rather than "double-stapling"[17], which installs two independent staples. Indeed, an *i, i+7* stitched all-hydrocarbon crosslink spanning four helical turns appeared especially well-suited to GLP-1 peptide design based upon the single *i, i+7* staple scanning SAR results.

To generate *i, i+7*-stitched constructs corresponding to the pairs of singly stapled residues located along a contiguous face of the GLP-1 helix, we installed from C-terminus to N-terminus an S-octenyl alanine (S8), a bis-pentenyl glycine (Bis-5), and an R-octenyl alanine (R8), to afford compatible *i, i+7* stapling between the olefins of S8-R5 and S5-R8 non-natural amino acid pairs within the peptide sequence (Figure 2a). Because Ala8-Glu9 is well known to be a dipeptidyl peptidase 4 (DPP4) proteolytic site, which is largely responsible for the clearance of circulating GLP-1, we replaced Ala with either glycine (G) or aminoisobutyric acid (J) in the stitched library (Figure 2b, Supplementary Table 1).[4] Comparing the activity of single and stitched compounds in the GLP-1R internalization assay, single staples were generally less disruptive to internalization (Figure 1e), whereas the SAR was more restrictive for the stitched analogs (Figure 2c, Supplementary Figure 2). Importantly, those stitches that successfully recapitulated the internalization activity of the unstapled control peptide were predominantly localized to the non-interacting face of the GLP-1 helix (Figure 2c, Supplementary Figure 2). If one of the two *i, i+7* staples was disfavored as a single-stapled construct, stitching could not salvage the activity and the influence of the disruptive stapled prevailed. In the case where the single *i, i+7* staples were tolerated on the interacting face (e.g. 19,26 and 26,33), stitching these pairs was not favorable (Figure 2b–c, Supplementary Figure 2). However, if individual staples were tolerated and localized to the non-interacting surface (e.g. 16,23 and 23,30), the stitched peptides retained favorable activity (Figure 2b–c, Supplementary Figure 2). The constructs that best preserved the biological properties of wild-type GLP-1 in the receptor internalization assay contained the 16,23,30 stitch (Figure 2c–d), and since the A8J peptides

were generally more active than the corresponding A8G analogs based on the dose-responsive analysis (0.15–5 μM), we selected SAH-GLP-1-A8J(16,23,30) as our lead construct for further testing. In advance of subjecting SAH-GLP-1- A8J(16,23,30) to a battery of conformational, proteolytic, and *in vivo* assays, we first confirmed that, in addition to functioning as an agonist in our screening GLP-1R binding and internalization assay, SAH-GLP-1-A8J(16,23,30) was capable of increasing cAMP levels in a gold standard GLP-1R signal transduction assay. We treated GLP-1R expressing CHO-K1 cells with a serial dilution of SAH-GLP-1-A8J(16,23,30) and observed dose-responsive cAMP induction (EC50, 160 pM), as detected by cAMP Hunter eXpress luminescence assay (Supplementary Figure 3).

We next examined the impact of the installed *i, i+7* stitch on the secondary structure of the template GLP-1 peptide, as assessed by circular dichroism (CD), which measures average conformation in solution. Indeed, SAH-GLP-1-A8J(16,23,30) and the corresponding peptides bearing the individual *i, i+7* staple components, SAH-GLP-1-A8J (16,23) and (23,30), recapitulated the α-helicity of GLP-1 (Figure 3a). To probe comparative structural dynamics, we analyzed the peptide panel by hydrogen-deuterium exchange mass spectrometry (HXMS), which detects changes in peptide or protein conformation over time based on differences in hydrogen-bonding and solvent exposure[46]. After 10 sec of D2O exposure, GLP-1 peptides bearing single or stitched *i,i+7* staples showed reduced deuterium exchange by 2.4–3 fold compared to the template peptide (Figure 3b), highlighting the conformational rigidity conferred by the staples and a structure-dynamics relationship not detectable by CD averaging. Furthermore, monitoring deuterium exchange over time revealed that *i, i+7* stitching consistently conferred more protection at 3 min, 25 min, and 60 min when compared to single *i, i+7* stapling alone (Figure 3b).

To evaluate the potential benefit of stitching in maximizing protease resistance, we subjected SAH-GLP-1-A8J(16,23,30), its single-stapled analogs, and the unstapled GLP-1 peptide to proteolytic digestion by proteinase K, a broad-spectrum protease that hydrolyzes the peptide bond adjacent to the carboxyl group of hydrophobic amino acids. As expected, the control GLP-1 peptide was rapidly digested *in vitro* with a half-life of less than 10 minutes (Figure 3c). The single *i, i+7* staples showed 3- to 13-fold improvement compared to wild-type, with respective half-lives of 120 and 30 minutes for SAH-GLP-1-A8J(16,23) and SAH-GLP-1-A8J(23,30). The stitched peptide was the most proteolytically resistant construct, with a remarkable half-life of 220 minutes that bested the control peptide by over 24-fold and the singly-stapled peptides by 2–7 fold (Figure 3c). Notably, among the conformational analyses performed, proteolysis best distinguished between the 4 peptides, with the more N-terminal *i, i+7* staple providing the greatest benefit among the single-stapled peptides and *i, i+7* stitching yielding the most stable, proteolytic resistant construct overall.

We next determined whether the relative structural and proteolytic stability of SAH-GLP-1-A8J(16,23,30) translated into a functional benefit *in vivo*. We performed glucose tolerance tests (GTT) in B6 mice (n=8 per condition) fasted overnight, administering the corresponding panel of peptides at 10 nmol/kg IP followed by a glucose bolus (2g/kg) 30 minutes later, and monitored glucose clearance over time (Figure 3d). In accordance with the hierarchy defined by protease resistance testing, wild-type GLP-1 and SAH-GLP-1-

A8J(23,30) were the least effective at improving glucose tolerance, whereas SAH-GLP-1-A8J(16,23,30) followed by SAH-GLP-1-A8J(16,23) produced the greatest reduction in blood glucose excursions. Indeed, SAH-GLP-1-A8J(16,23,30) lowered the maximum serum glucose concentration by nearly half of the vehicle control, and achieved euglycemia within 60 minutes of the glucose bolus.

The favorable activity profile of SAH-GLP-1-A8J(16,23,30) motivated us to compare its activity to the FDA-approved GLP-1 analog semaglutide[3] in Leprdb mice, which exhibit fasting hyperglycemia. Whereas the *in vivo* stability of semaglutide was optimized based on mutating the DPP4 proteolytic site and appending a lipid moiety to maximize albumin binding[3], here we instead combined DPP4 site mutagenesis with structural reinforcement by *i, i+7* stitching, which confers direct resistance to proteolysis (Figure 3c, Supplementary Figure 4). Both approaches result in marked improvements in comparative *ex vivo* mouse plasma stability testing, yielding half-lives 12-fold (semaglutide) and 23-fold (SAH-GLP-1-A8J[16,23,30)]) greater than the natural GLP-1 peptide (Figure 4a). Single IP injection (10 nmol/kg) of SAH-GLP-1-A8J(16,23,30) produced a more rapid, initial reduction in serum glucose compared to semaglutide, with both compounds sustaining a similar 2–2.5 fold reduction in glucose level compared to vehicle and wild-type GLP-1 for the 12-hour duration of the experiment (Figure 4b–c).

CONCLUSION

In summary, we demonstrate that a staple-scanning and stitching approach can produce a structurally-stabilized and protease-resistant GLP-1R agonist with promising therapeutic activity in mouse models. Comparative conformational analyses of GLP-1 and its single-stapled and stitched variants revealed that HXMS was more effective than circular dichroism at identifying differences in structural stabilization. *In vitro* proteolysis testing was the most sensitive method for detecting the differential impact of staple variants on structural stability, and revealed the superior proteolytic resistance of *i, i+7* stitching. Indeed, the peptide hierarchy determined by *in vitro* protease resistance testing matched that of anti-hyperglycemic activity *in vivo*. Our data suggest that, for the appropriate template, stitching could be a valuable alternative approach to designing lengthy, α-helical peptides with drug-like properties.

EXPERIMENTAL SECTION

Peptide synthesis.

All-hydrocarbon stapled peptides were synthesized using Rink Amide AM resin (Merck) with a free N terminus nd purified to >95% homogeneity by LC/MS as previously described[47] (Supplementary Figure 5, Supplementary Table 1). The *i, i+7* staple scan was synthesized using (R)-N-Fmoc-α-(7-octenyl)alanine and (S)-N-Fmoc-α-(4-pentenyl)alanine at the N- and C-terminal positions, respectively. The stitched peptides were synthesized using, from N- to C-terminal positions, (R)-N-Fmoc-α-(7-octenyl)alanine, N-Fmoc-α,α-Bis(4-pentenyl) glycine, and (S)-N-Fmoc-α-(7-octenyl)alanine (Nagase).

Cell culture.

U2OS cells were stably reconstituted with human GLP-1 receptor (GenBank Acc. NM_002062) fused to the N-terminus of enhanced green fluorescent protein (EGFP) and continuous expression maintained by treatment with 0.5 mg/mL G418 in DMEM supplemented with 2 mM L-Glutamine, 1% penicillin-streptomycin, and 10% FBS). Cells were verified to be mycoplasma-free using the MycoAlert mycoplasma detection kit (Lonza Biologics Inc).

High content receptor internalization assay.

For high-content epifluorescence microscopy analysis, cells were plated in black, clear-bottom 384-well plates overnight at a density of 4×10^3 cells per well. The following day, the cells were exposed to fresh media containing Hoechst 33342 (1:5000 dilution of 10 mg/mL) and treated with the indicated peptide dosing at 37 °C for 1 h followed by ImageXpress Microscopy imaging. For each treatment condition, performed in technical quadruplicate, data were collected at one central site per well at 10× magnification, followed by analysis and quantitation for internalized receptor foci using MetaXpress software. For each comparative analysis, all stapled peptides in the panel were measured on the same day using the same plating of cells and peptide dilutions. The entire experiment was then repeated on different days using freshly plated cells and peptide dilutions.

cAMP assay.

Cyclic AMP production was measured using the cAMP Hunter™ eXpress GLP1R CHO-K1 GPCR Assay according to the manufacturer's instructions (Eurofins, 95–0062E2CP2S). Briefly, the frozen cells were thawed and plated in 96 well format for overnight incubation at 37°C in a humidified incubator, with the top two rows of the plate reserved for the cAMP standard. To generate the standard curve, the cAMP standard was diluted to achieve an initial concentration of 2.3 μM and then serially diluted 1:3 until reaching a final dose of 39 pM. SAH-GLP-1-A8J(16,23,30) was diluted to achieve a starting concentration of 3.7 nM and serially diluted 1:3 to reach a final dose of 0.56 pM. The generated SAH-GLP-1-A8J(16,23,30) dilutions were then added to the plated cells and allowed to incubate at 37°C for 30 min. After workup with lysis buffer and cAMP antibody incubation per the manufacturer's protocol, luminescence was read on a SpectraMax M5 micro-plate reader (Molecular Devices) at equilibrium. Nonlinear regression analysis was performed using Prism software (GraphPad) to obtain EC50s for the cAMP standard curve and cAMP induction by SAH-GLP-1-A8J(16,23,30).

Circular dichroism spectroscopy.

Peptides were dissolved in 25% acetonitrile/water to achieve a concentration of 50 μM. Circular dichroism (CD) spectra were obtained on a spectropolarimeter (Aviv) using standard measurement parameters of temperature, 25°C; wavelength, 190–260 nm; step resolution, 0.5 nm; speed, 20 nm min–1; accumulations, 10.

Hydrogen deuterium exchange mass spectrometry.

For analysis of exchange into the indicated GLP-1 constructs, the peptides were dissolved in 25% acetonitrile/water at 50 μM and kept on ice. Deuterium labeling was initiated with an 18-fold dilution into D2O buffer (10 mM potassium phosphate pD 7.01, 100 mM NaCl) at 21°C. After 10 seconds of labeling, the reaction was quenched with the addition of an equal volume of quenching buffer (150 mM sodium phosphate pH 2.48) at 0°C. Samples were then injected onto an in-house packed POROS 20-R2 trap for peptide trapping and desalting for 3 minutes. A Waters nanoACQUITY LC was used to elute each peptide from the trap with a 15%–70% gradient of acetonitrile over 6 minutes at a flow rate of 100 μL/min. Eluant was directed into a Waters Xevo G2 mass spectrometer operated in TOF-only mode for mass analysis. Data were analyzed as described[31]. All mass spectra were processed manually using MagTran. The relative amount of deuterium in the GLP-1 constructs was determined by subtracting the centroid mass of the undeuterated form from the deuterated form, at each condition. Deuterium levels were not corrected for back exchange and thus reported as relative.

Peptide proteolysis assay.

In vitro proteolytic degradation was measured by LC/MS (Agilent 1200) using the following parameters: 20 μl injection, 0.6 mL flow rate, 20-min run time consisting of a gradient of water (0.1% formic acid) to 20%–80% acetonitrile (0.75% formic acid) over 15-min, 4-min wash to revert to starting gradient conditions, and 0.5-min post-time. The DAD signal was set to 280 nm with an 8-nm bandwidth and MSD set to scan mode with one channel at (M +2H)/2, ± 1 mass units, and the other at (M+3H)/3, ± 1 mass units. Integration of each MSD signal yielded areas under the curve of >108 counts. Reaction samples were composed of 5 μl peptide in DMSO (1 mM stock) and 195 μl buffer consisting of 50 mM Tris HCl, pH 7.4. Upon injection of the zero-time sample, 2.5 μl of 100 ng/μL proteinase K (New England Biolabs) was added, and the amount of intact peptide quantitated by serial injection over time. A plot of MSD area versus time yielded an exponential decay curve, and half-lives were determined by nonlinear regression analysis using Prism software (GraphPad).

Plasma stability testing.

Peptide stability was tested in freshly drawn mouse plasma collected in lithium heparin tubes. Peptide-plasma incubations were set up with 500 μl of plasma spiked with 10 μM of the individual peptides. Samples were gently shaken in an orbital shaker at 37°C and 20 μl aliquots were removed at 0, 5, 15, 30, 60, 120 and 200 min and added to 150 μl of a mixture containing 50% water:50% acetonitrile to stop further degradation of the peptides. The samples were allowed to sit on ice for the duration of the assay and then transferred to a MultiScreen Solvinert 0.45 μm low-binding hydrophilic PTFE plate (Millipore). The filtrate was directly analyzed by LC/MS/MS using a Thermo BetaSil column, 2.1×50 mm, 5 μm. The peptides were detected on a Sciex 6500 Qtrap mass spectrometer as 3+ or 4+ charged ions using the following mass transitions: 824.9 to 571.3 for GLP-1, 1029 to 690 for semaglutide, and 878.6 to 571.2 for SAH-GLP-1-A8J(16,23,30). The percentage of remaining peptide was determined by the decrease in chromatographic peak area and log transformed to calculate the half-life.

In vivo efficacy testing of SAH-GLP-1 peptides.

Male B6 and db/db mice (JAX 000697) at 10–12 weeks of age were housed (5 mice/cage) at a constant room temperature of 24°C on a normal day-light cycle and provided a standard diet *ad libitum*. After one week of acclimatization, B6 mice (n=8 per treatment arm) were fasted for 16 hours overnight and the following morning baseline blood glucose levels were measured (Onetouch), followed by intraperitoneal (IP) injection of vehicle (saline) or the indicated peptide (10 nmol/kg). Thirty minutes later, the mice were treated with a bolus IP injection of glucose (2 g/kg, 20% aqueous solution), followed by serial blood glucose monitoring at 0, 15, 30, 60, and 120 min. To evaluate the comparative anti-hyperglycemic effects of peptides in db/db mice (n=8 per treatment arm), vehicle (saline) or the indicated peptide (10 nmol/kg) was injected IP and blood glucose levels monitored at 0, 15, 30, 60, and 720 min in *ad libitim* fed mice. Samples for the measurement of blood glucose were obtained from the tail tip capillary, collected into heparinized capillary tubes. All animal experiments were approved by and performed in accordance with the guidelines and regulations set forth by the Institutional Animal Care and Use Committee of the Dana-Farber Cancer Institute.

Supplementary Material

Refer to Web version on PubMed Central for supplementary material.

Acknowledgments

We thank T. Oo for peptide synthesis and E. Smith for assistance with figure preparation. We dedicate this work to the memory of S. Rudnicki, whose guidance was central to the success of so many projects at the ICCB-Longwood Screening Facility of Harvard Medical School, including our high-content epifluorescence microscopy receptor-internalization analyses.

Funding Sources

This research was supported by NIH grant R35CA197583 and a Leukemia and Lymphoma Society (LLS) Scholar Award to L.D.W., NIH grant R50CA211399 to G.H.B., a Juvenile Diabetes Research foundation (JDRF) postdoctoral fellowship to A.F. and NIH grant R01DK078081, and a Barry and Mimi Sternlicht Type 1 Diabetes Research Fund grant and JDRF grant 2-SRA-2015-58-Q-R, to N.N.D. Additional support was provided by a research collaboration between J.R.E. and the Waters Corporation.

ABBREVIATIONS USED

SAH	Stabilized Alpha-Helix
GLP-1	Glucagon-like Peptide 1
GLP-1R	Glucagon-Like Peptide 1 Receptor
DPP4	Dipeptidyl Peptidase 4

REFERENCES

(1). Drucker DJ, and Nauck MA (2006) The incretin system: glucagon-like peptide-1 receptor agonists and dipeptidyl peptidase-4 inhibitors in type 2 diabetes, Lancet 368, 1696–1705. [PubMed: 17098089]

(2). Drucker DJ (2006) The biology of incretin hormones, Cell Metab 3, 153–165. [PubMed: 16517403]

(3). Lau J, Bloch P, Schaffer L, Pettersson I, Spetzler J, Kofoed J, Madsen K, Knudsen LB, McGuire J, Steensgaard DB, Strauss HM, Gram DX, Knudsen SM, Nielsen FS, Thygesen P, Reedtz-Runge S, and Kruse T (2015) Discovery of the Once-Weekly Glucagon-Like Peptide-1 (GLP-1) Analogue Semaglutide, J Med Chem 58, 7370–7380. [PubMed: 26308095]

(4). Deacon CF, Knudsen LB, Madsen K, Wiberg FC, Jacobsen O, and Holst JJ (1998) Dipeptidyl peptidase IV resistant analogues of glucagon-like peptide-1 which have extended metabolic stability and improved biological activity, Diabetologia 41, 271–278. [PubMed: 9541166]

(5). Knudsen LB, Nielsen PF, Huusfeldt PO, Johansen NL, Madsen K, Pedersen FZ, Thogersen H, Wilken M, and Agerso H (2000) Potent derivatives of glucagon-like peptide-1 with pharmacokinetic properties suitable for once daily administration, J Med Chem 43, 1664–1669. [PubMed: 10794683]

(6). Lee SH, Lee S, Youn YS, Na DH, Chae SY, Byun Y, and Lee KC (2005) Synthesis, characterization, and pharmacokinetic studies of PEGylated glucagon-like peptide-1, Bioconjugate Chem 16, 377–382.

(7). Miranda LP, Winters KA, Gegg CV, Patel A, Aral J, Long JS, Zhang JW, Diamond S, Guido M, Stanislaus S, Ma M, Li HY, Rose MJ, Poppe L, and Veniant MM (2008) Design and synthesis of conformationally constrained glucagon-like peptide-1 derivatives with increased plasma stability and prolonged in vivo activity, J Med Chem 51, 2758–2765. [PubMed: 18412318]

(8). Murage EN, Gao GZ, Bisello A, and Ahn JM (2010) Development of Potent Glucagon-like Peptide-1 Agonists with High Enzyme Stability via Introduction of Multiple Lactam Bridges, J Med Chem y 53, 6412–6420.

(9). Johnson LM, Barrick S, Hager MV, McFedries A, Homan EA, Rabaglia ME, Keller MP, Attie AD, Saghatelian A, Bisello A, and Gellman SH (2014) A Potent alpha/beta-Peptide Analogue of GLP-1 with Prolonged Action in Vivo, J Am Chem Soc 136, 12848–12851. [PubMed: 25191938]

(10). Sebokova E, Christ AD, Wang HY, Sewing S, Dong JZ, Taylor J, Cawthorne MA, and Culler MD (2010) Taspoglutide, an Analog of Human Glucagon-Like Peptide-1 with Enhanced Stability and in Vivo Potency, Endocrinol 151, 2474–2482.

(11). Green BD, Gault VA, Mooney MH, Irwin N, Harriott P, Greer B, Bailey CJ, Oharte FPM, and Flatt PR (2004) Degradation, receptor binding, insulin secreting and antihyperglycaemic actions of palmitatederivatised native and Ala(8)-substituted GLP-1 analogues, Biol Chem 385, 169–177. [PubMed: 15101559]

(12). Denton EV, Craig CJ, Pongratz RL, Appelbaum JS, Doerner AE, Narayanan A, Shulman GI, Cline GW, and Schepartz A (2013) A beta-Peptide Agonist of the GLP-1 Receptor, a Class B GPCR, Org Lett 15, 5318–5321. [PubMed: 24087900]

(13). DeFronzo RA, Ratner RE, Han J, Kim DD, Fineman MS, and Baron AD (2005) Effects of exenatide (exendin-4) on glycemic control and weight over 30 weeks in metformin-treated patients with type 2 diabetes, Diabetes Care 28, 1092–1100. [PubMed: 15855572]

(14). Schafmeister CE, Po J, and Verdine GL (2000) An All-Hydrocarbon Cross-Linking System for Enhancing the Helicity and Metabolic Stability of Peptides, J Am Chem Soc 122, 5891–5892.

(15). Walensky LD, Kung AL, Escher I, Malia TJ, Barbuto S, Wright RD, Wagner G, Verdine GL, and Korsmeyer SJ (2004) Activation of apoptosis in vivo by a hydrocarbon-stapled BH3 helix, Science 305, 1466–1470. [PubMed: 15353804]

(16). Danial NN, Walensky LD, Zhang CY, Choi CS, Fisher JK, Molina AJA, Datta SR, Pitter KL, Bird GH, Wikstrom JD, Deeney JT, Robertson K, Morash J, Kulkarni A, Neschen S, Kim S, Greenberg ME, Corkey BE, Shirihai OS, Shulman GI, Lowell BB, and Korsmeyer SJ (2008) Dual role of proapoptotic BAD in insulin secretion and beta cell survival, Nature Medicine 14, 144–153.

(17). Bird GH, Madani N, Perry AF, Princiotto AM, Supko JG, He X, Gavathiotis E, Sodroski JG, and Walensky LD (2010) Hydrocarbon double-stapling remedies the proteolytic instability of a lengthy peptide therapeutic, Proc Natl Acad Sci U S A 107, 14093–14098. [PubMed: 20660316]

(18). LaBelle JL, Katz SG, Bird GH, Gavathiotis E, Stewart ML, Lawrence C, Fisher JK, Godes M, Pitter K, Kung AL, and Walensky LD (2012) A stapled BIM peptide overcomes apoptotic resistance in hematologic cancers, J Clin Invest 122, 2018–2031. [PubMed: 22622039]

(19). Bird GH, Boyapalle S, Wong T, Opoku-Nsiah K, Bedi R, Crannell WC, Perry AF, Nguyen H, Sampayo V, Devareddy A, Mohapatra S, Mohapatra SS, and Walensky LD (2014) Mucosal delivery of a doublestapled RSV peptide prevents nasopulmonary infection, J Clin Invest 124, 2113–2124. [PubMed: 24743147]

(20). Ljubicic S, Polak K, Fu A, Wiwczar J, Szlyk B, Chang YG, Alvarez-Perez JC, Bird GH, Walensky LD, Garcia-Ocana A, and Danial NN (2015) Phospho-BAD BH3 Mimicry Protects beta Cells and Restores Functional beta Cell Mass in Diabetes, Cell Reports 10, 497–504. [PubMed: 25640178]

(21). Bernal F, Tyler AF, Korsmeyer SJ, Walensky LD, and Verdine GL (2007) Reactivation of the p53 tumor suppressor pathway by a stapled p53 peptide, j Am Chem Soc 129, 2456–2457. [PubMed: 17284038]

(22). Bernal F, Wade M, Godes M, Davis TN, Whitehead DG, Kung AL, Wahl GM, and Walensky LD (2010) A stapled p53 helix overcomes HDMXmediated suppression of p53, Cancer Cell 18, 411–422. [PubMed: 21075307]

(23). Chang YS, Graves B, Guerlavais V, Tovar C, Packman K, To KH, Olson KA, Kesavan K, Gangurde P, Mukherjee A, Baker T, Darlak K, Elkin C, Filipovic Z, Qureshi FZ, Cai HL, Berry P, Feyfant E, Shi XGE, Horstick J, Annis DA, Manning AM, Fotouhi N, Nash H, Vassilev LT, and Sawyer TK (2013) Stapled alpha-helical peptide drug development: A potent dual inhibitor of MDM2 and MDMX for p53-dependent cancer therapy, Proc Natl Acad U S A 110, E3445–E3454.

(24). Carvajal LA, Ben Neriah D, Senecal A, Benard L, Thiruthuvanathan V, Yatsenko T, Narayanagari SR, Wheat JC, Todorova TI, Mitchell K, Kenworthy C, Guerlavais V, Annis DA, Bartholdy B, Will B, Anampa JD, Mantzaris I, Aivado M, Singer RH, Coleman RA, Verma A, and Steidl U (2018) Dual inhibition of MDMX and MDM2 as a therapeutic strategy in leukemia, Sci Transl Med 10, 12.

(25). Hilinski GJ, Kim YW, Hong J, Kutchukian PS, Crenshaw CM, Berkovitch SS, Chang A, Ham S, and Verdine GL (2014) Stitched alpha-Helical Peptides via Bis Ring-Closing Metathesis, J Am Chem Soc 136, 12314–12322. [PubMed: 25105213]

(26). Bird GH, Irimia A, Ofek G, Kwong PD, Wilson IA, and Walensky LD (2014) Stapled HIV-1 peptides recapitulate antigenic structures and engage broadly neutralizing antibodies, Nat Struct Mol Biol 21, 1058–1067. [PubMed: 25420104]

(27). Walensky LD, Pitter K, Morash J, Oh KJ, Barbuto S, Fisher J, Smith E, Verdine GL, and Korsmeyer SJ (2006) A stapled BID BH3 helix directly binds and activates BAX, Mol Cell 24, 199–210. [PubMed: 17052454]

(28). Stewart ML, Fire E, Keating AE, and Walensky LD (2010) The MCL-1 BH3 helix is an exclusive MCL-1 inhibitor and apoptosis sensitizer, Nat Chem Biol 6, 595–601. [PubMed: 20562877]

(29). Leshchiner ES, Braun CR, Bird GH, and Walensky LD (2013) Direct activation of full-length proapoptotic BAK, Proc Natl Acad Sci U S A 110, E986–E995. [PubMed: 23404709]

(30). Szlyk B, Braun CR, Ljubicic S, Patton E, Bird GH, Osundiji MA, Matschinsky FM, Walensky LD, and Danial NN (2014) A phospho-BAD BH3 helix activates glucokinase by a mechanism distinct from that of allosteric activators, Nat Struct Mol Biol 21, 36–42. [PubMed: 24317490]

(31). Barclay LA, Wales TE, Garner TP, Wachter F, Lee S, Guerra RM, Stewart ML, Braun CR, Bird GH, Gavathiotis E, Engen JR, and Walensky LD (2015) Inhibition of Pro-Apoptotic BAX by a Noncanonical Interaction Mechanism, Mol Cell 57, 873–886. [PubMed: 25684204]

(32). Guerra RM, Bird GH, Harvey EP, Dharia NV, Korshavn KJ, Prew MS, Stegmaier K, and Walensky LD (2018) Precision Targeting of BFL-1/A1 and an ATM Co-dependency in Human Cancer, Cell Reports 24, 3393–3403. [PubMed: 30257201]

(33). Escudero S, Zaganjor E, Lee S, Mill CP, Morgan AM, Crawford EB, Chen JH, Wales TE, Mourtada R, Luccarelli J, Bird GH, Steidl U, Engen JR, Haigis MC, Opferman JT, and Walensky LD (2018) Dynamic Regulation of Long-Chain Fatty Acid Oxidation by a Noncanonical Interaction between the MCL-1 BH3 Helix and VLCAD, Mol Cell 69, 729–743. [PubMed: 29499131]

(34). Araghi RR, Bird GH, Ryan JA, Jenson JM, Godes M, Pritz JR, Grant RA, Letai A, Walensky LD, and Keating AE (2018) Iterative optimization yields Mcl-1-targeting stapled peptides with selective cytotoxicity to Mcl-1-dependent cancer cells, Proc Natl Acad Sci U S A 115, E886–E895. [PubMed: 29339518]

(35). Edwards AL, Gavathiotis E, LaBelle JL, Braun CR, Opoku-Nsiah KA, Bird GH, and Walensky LD (2013) Multimodal Interaction with BCL-2 Family Proteins Underlies the Proapoptotic Activity of PUMA BH3, Chem Biol 20, 888–902. [PubMed: 23890007]

(36). Yang PY, Zou H, Chao E, Sherwood L, Nunez V, Keeney M, Ghartey-Tagoe E, Ding Z, Quirino H, Luo X, Welzel G, Chen G, Singh P, Woods AK, Schultz PG, and Shen W (2016) Engineering a longacting, potent GLP-1 analog for microstructure-based transdermal delivery, Proc Natl Acad Sci U S A 113, 4140–4145. [PubMed: 27035989]

(37). Yang PY, Zou HF, Lee C, Muppidi A, Chao E, Fu QW, Luo XZ, Wang DL, Schultz PG, and Shen WJ (2018) Stapled, Long-Acting Glucagon-like Peptide 2 Analog with Efficacy in Dextran Sodium Sulfate Induced Mouse Colitis Models, J Med Chem 61, 3218–3223. [PubMed: 29528634]

(38). Zhang L, Navaratna T, Liao J, and Thurber GM (2015) Dual-purpose linker for alpha helix stabilization and imaging agent conjugation to glucagon-like peptide-1 receptor ligands, Bioconjug Chem 26, 329–337. [PubMed: 25594741]

(39). Zhang L, Navaratna T, and Thurber GM (2016) A Helix-Stabilizing Linker Improves Subcutaneous Bioavailability of a Helical Peptide Independent of Linker Lipophilicity, Bioconjug Chem 27, 1663–1672. [PubMed: 27327034]

(40). Vilsboll T, Brock B, Perrild H, Levin K, Lervang HH, Kolendorf K, Krarup T, Schmitz O, Zdravkovic M, Le-Thi T, and Madsbad S (2008) Liraglutide, a oncedaily human GLP-1 analogue, improves pancreatic B-cell function and arginine-stimulated insulin secretion during hyperglycaemia in patients with Type 2 diabetes mellitus, Diabetic Medicine 25, 152–156. [PubMed: 18201212]

(41). Gutniak M, Orskov C, Holst JJ, Ahren B, and Efendic S (1992) Antidiabetogenic Effect of Glucagon-like Peptide-1 (7–36)amide in Normal Subjects and Patients With Diabetes-mellitus, New Eng J Med 326, 1316–1322. [PubMed: 1348845]

(42). Ahmann AJ, Capehorn M, Charpentier G, Dotta F, Henkel E, Lingvay I, Holst AG, Annett MP, and Aroda VR (2018) Efficacy and Safety of Once-Weekly Semaglutide Versus Exenatide ER in Subjects With Type 2 Diabetes (SUSTAIN 3): A 56-Week, Open-Label, Randomized Clinical Trial, Diabetes Care 41, 258–266. [PubMed: 29246950]

(43). Underwood CR, Garibay P, Knudsen LB, Hastrup S, Peters GH, Rudolph R, and Reedtz-Runge S (2010) Crystal Structure of Glucagon-like Peptide-1 in Complex with the Extracellular Domain of the Glucagon-like Peptide-1 Receptor, J Biol Chem 285, 723–730. [PubMed: 19861722]

(44). Jazayeri A, Rappas M, Brown AJH, Kean J, Errey JC, Robertson NJ, Fiez-Vandal C, Andrews SP, Congreve M, Bortolato A, Mason JS, Baig AH, Teobald I, Doré AS, Weir M, Cooke RM, and Marshall FH (2017) Crystal structure of the GLP-1 receptor bound to a peptide agonist, Nature 546, 254. [PubMed: 28562585]

(45). Song GJ, Yang DH, Wang YX, de Graaf C, Zhou QT, Jiang SS, Liu KW, Cai XQ, Dai AT, Lin GY, Liu DS, Wu F, Wu YR, Zhao SW, Ye L, Han GW, Lau J, Wu BL, Hanson MA, Liu ZJ, Wang MW, and Stevens RC (2017) Human GLP-1 receptor transmembrane domain structure in complex with allosteric modulators, Nature 546, 312–315. [PubMed: 28514449]

(46). Engen JR (2009) Analysis of protein conformation and dynamics by hydrogen/deuterium exchange MS, Anal Chem 81, 7870–7875. [PubMed: 19788312]

(47). Bird GH, Mazzola E, Opoku-Nsiah K, Lammert MA, Godes M, Neuberg DS, and Walensky LD (2016) Biophysical determinants for cellular uptake of hydrocarbon-stapled peptide helices, Nat Chem Biol 12, 845–852. [PubMed: 27547919]

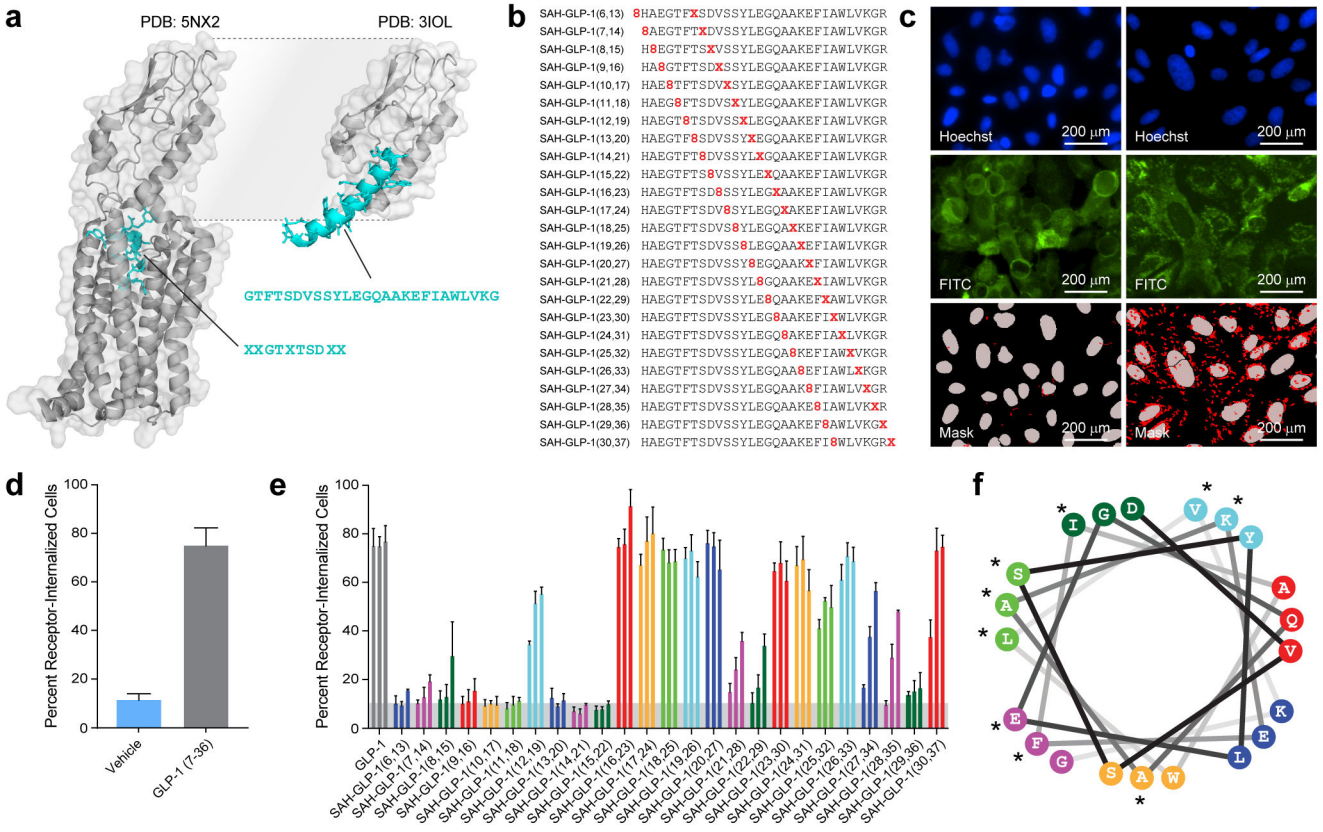

Figure 1.

An *i, i+7* staple scan of GLP-1 reveals a distinctive structure-activity relationship for crosslink placement. (a) Structures of GLP-1 in complex with GLP-1R demonstrating the burial of the peptide's N-terminus (PDB: 5NX2) (left) and its helix-in-groove interaction with the extracellular domain of GLP-1R (PDB: 3IOL) (right). (b) Amino acid sequences of an *i, i+7* staple scanning library of GLP-1. 8, R-octenyl alanine; X, S-pentenyl alanine. (c) GFP-GLP-1R expressing U2OS cells demonstrate fluorescence of the plasma membrane at baseline (left), but upon GLP-1 peptide exposure (right) undergo receptor internalization, which is reflected by fluorescent cytosolic punctae that can be quantified by high-content epifluorescence imaging. Hoechst 33342 stained nuclei, blue; GFP-GLP-1R, green; binary mask showing nuclei (grey) and vesicles containing internalized GFP-GLP-1R (red). (d) The percentage of cells containing internalized GFP-GLP-1R under each condition (vehicle vs. 0.625 μM GLP-1) is shown in the bar graph. Data are mean ± s.d. for experiments done in technical quadruplicate and performed twice with similar results. (e) Percentage of U2OS cells with internalized GLP-1R in response to treatment with differentially *i, i+7*-stapled GLP-1 peptides (10, 2.5, 0.625 μM, from right to left). Data are mean ± s.d. for experiments done in technical quadruplicate and performed at least twice with similar results. (f) Helical wheel depiction of GLP-1 (aa 15–35), colored by the locations of sequential pairs of *i, i+7* staples along the length of the peptide helix (e.g. red: 16,23 and 23,30; orange: 17,24 and 24,31, etc.). Residues that engage in direct interactions with GLP-1R are marked by an asterisk.

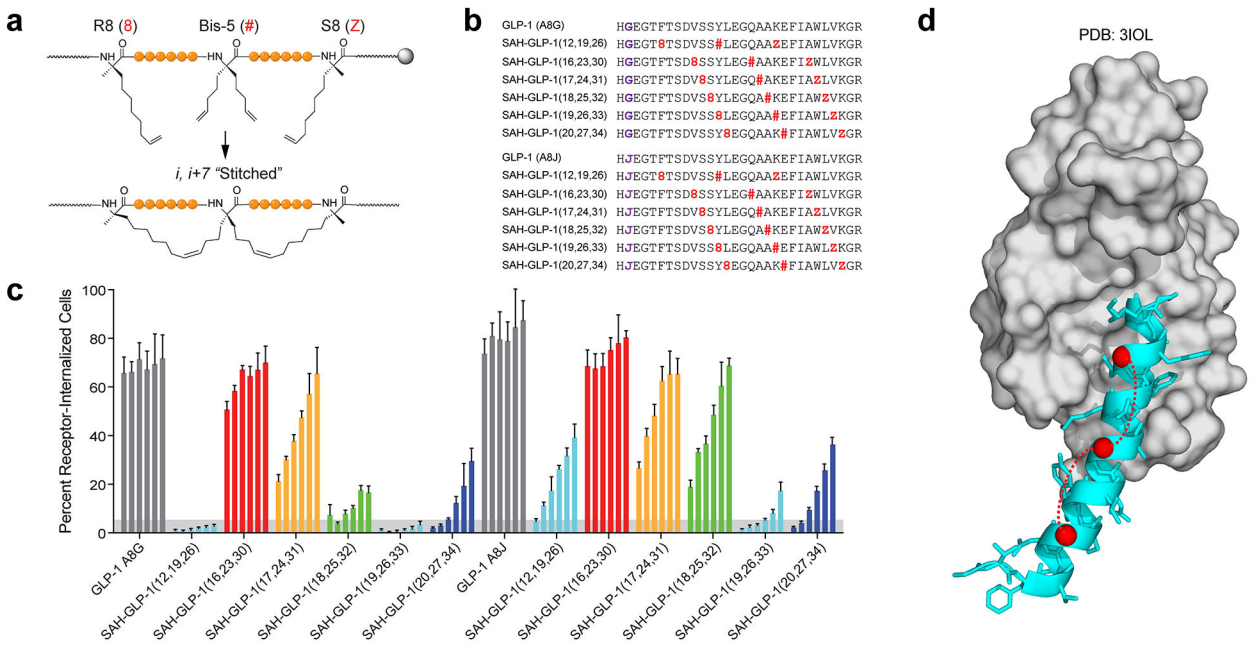

Figure 2.

Design and functional testing of *i, i+7*-stitched GLP-1 peptides. (a) Synthesis of *i, i+7*-stitched peptides by insertion, from C-terminus to N-terminus, S-octenyl alanine, bis-pentenyl glycine, and R-octenyl alanine at sequential *i, i+7* positions within the GLP-1 peptide template. (b) Amino acid sequences of double *i, i+7*-stitched peptides. Ala8 was replaced by Gly (G) or Aib (J) to prevent DPP4 proteolysis at this site. 8, R-octenyl alanine; #, bis-pentenyl glycine; Z, S-octenyl alanine. (c) Percentage of U2OS cells with internalized GLP-1R in response to treatment with differentially *i, i+7*-stitched GLP-1 peptides (serial dilution from 5 to 0.15 μM, from right to left). Data are mean ± s.d. for experiments done in technical quadruplicate and performed at least twice with similar results. A8G, left series; A8J, right series. (d) Helix-in-groove depiction of the complex between GLP-1 (aa 10–35; cyan) and the extracellular domain of GLP-1R (grey). The stitch that best preserves the biological activity of GLP-1 (16,23,30; schematized in red) is localized on the helical surface opposite to the binding interface.

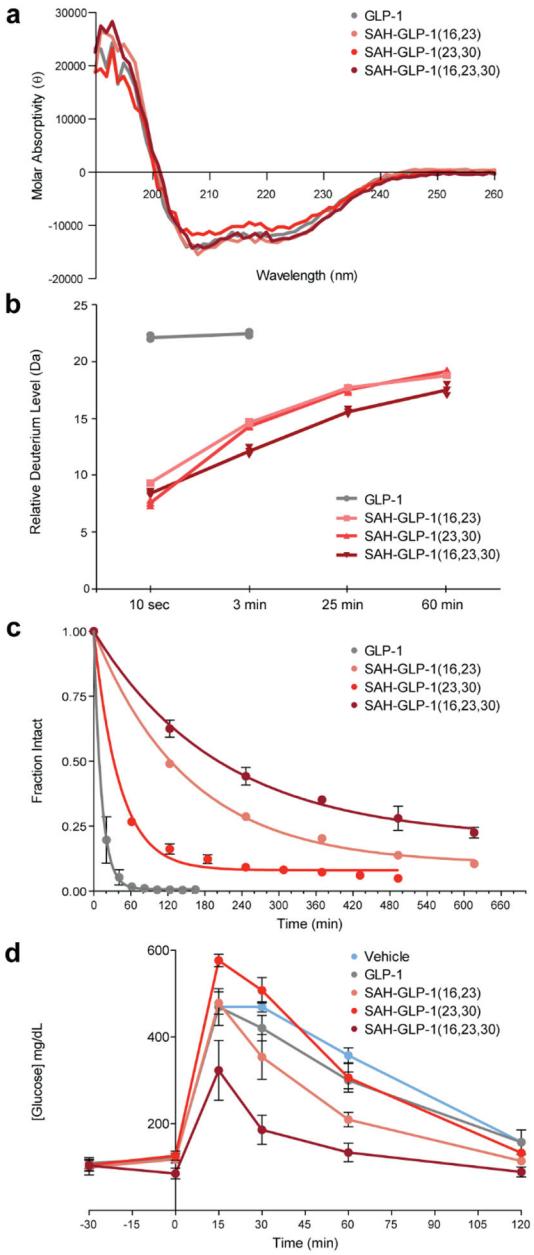

Figure 3.

Conformational stability, protease resistance and anti-hyperglycemic activity of differentially stapled GLP-1 peptides. (a) CD of SAH-GLP-1-A8J(16,23,30), its single-stapled analogs, and GLP-1. (b) HXMS of the 4-peptide panel performed in triplicate at the indicated deuterium labeling time points. (c) Proteinase K digestion and intact peptide quantified over time by LC/MS. Data are mean ± s.d. for experiments performed in triplicate. t1/2 = 9, 120, 30, and 220 min, for GLP-1 and SAH-GLP-1-A8J (16, 23), (23,30), and (16,23,30), respectively. (d) GTT after overnight fast for the indicated peptides or vehicle (10 nmol/kg IP dosing) followed by glucose (2 g/kg IP) 30 min later. Data are mean ± s.e.m. for serum glucose values measured over time in n=8 6 mice per treatment condition.

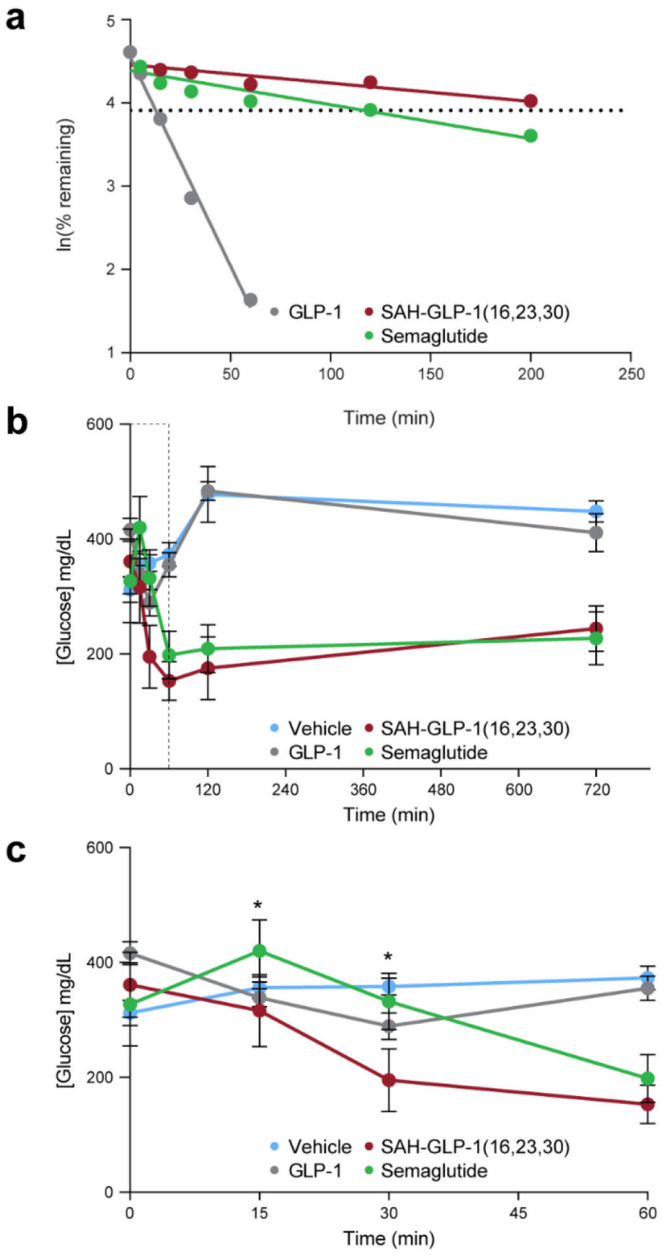

Figure 4.

Comparative plasma stability and glycemic control testing of SAH-GLP-1-A8J(16,23,30) and semaglutide. (a) *Ex vivo* mouse plasma stability testing of GLP-1, SAH-GLP-1-A8J(16,23,30), and semaglutide revealed half-lives of 14, 320, and 170 min, respectively. Dotted line, ln(50%). (b) Diabetic Leprdb mice were treated with a single 10 nmol/kg IP dose of GLP-1, SAH-GLP-1-A8J(16,23,30), semaglutide or vehicle control, followed by serum glucose monitoring over 12 hours. Data are mean ± s.e.m. for n=8 mice per treatment condition. (c) The region between 0 and 60 minutes is expanded to better visualize the data at early time points. *, SAH-GLP-1-A8J(16,23,30) vs. semaglutide: 15 min, p=0.0032; 30 min, p=0.0001.